RSC Advances

PAPER

View Article Online
View Journal | View Issue



Cite this: *RSC Adv.*, 2020, **10**, 24255

# Multicomponent gas separation and purification using advanced 2D carbonaceous nanomaterials†

Sayyed Jalil Mahdizadeh *[ab] and Elaheh K. Goharshadi[b]

Multicomponent gas separation and purification is an important pre- or post-processing step in industry. Herein, we employed a multiscale computational approach to investigate the possibility of multicomponent low-weight gas ($H_2$, $O_2$, $N_2$, $CO_2$, $CH_4$) separation and purification using novel porous 2D carbonaceous nanomaterials, namely Graphdiyne (GD), Graphenylene (GN), and Rhombic-Graphyne (RG). The dispersion-corrected plane-wave density functional theory (DFT) calculation combined with the Climbing Image Nudged Elastic Band (CI-NEB) method was employed to study the gas/membrane interaction energy and diffusion barrier of different gases passing through the geometrically optimized membranes. The results from CI-NEB calculations were then fitted to the Morse potential function to construct a bridge between quantum mechanics calculations and non-equilibrium molecular dynamics (NEMD) simulation. The selectivity of each membrane for all binary mixtures was calculated using the estimated diffusion energy barriers based on the Arrhenius equation. Finally, a series of extensive NEMD simulations were carried out to evaluate the real word and time dependent separation process. According to the results, $CH_4$ molecules can be completely separated from the other gases using a GD membrane, $O_2$ molecules from $CH_4$, $N_2$, and $CO_2$ by a GN membrane, and $H_2$ molecules from all other gases using a RG membrane.

Received 13th May 2020
Accepted 16th June 2020

DOI: 10.1039/d0ra04286b

rsc.li/rsc-advances



## Introduction

Multicomponent gas separation and purification is a vital pre- or post-processing step in many applications from large scale industrial ones to laboratorial low scale experiments.[1] From the practical point of view, the efficient separation of low weight gases ($H_2$, $O_2$, $N_2$, $CO_2$, $CH_4$) is of great significance because many of the light gases are feeds for many industrial processes.[1] For instance, $H_2$ can be separated from the other ingredients of syngas (CO and $CO_2$) to employ it as a green energy carrier with zero environmental footprint.[2] $O_2$ separation from the air is strongly encouraged by exponentially increasing demands in medical and industrial sectors.[3] $CO_2$ is one of the most significant greenhouse gases that is emitted to the Earth's atmosphere as a consequence of the world's dependence on fossil fuels which leads to severe climate changes and global warming.[2] Therefore, $CO_2$ capture, separation, and recycling from the combustion products of fossil fuels have great advantages for environment and related industries.[4] In natural gas sweetening process, $CH_4$ molecules separate from other contaminants such as $CO_2$ and $H_2S$.[5] $N_2$ is an important gas which is widely used as inert atmosphere in air-sensitive chemical reactions and cooling media because of its suitably low boiling point (77.3 K).[6]

Among various gas separation methods, membrane technique provides several advantages such as high energy efficiency, facile operation, easy maintenance, and low investment cost.[7] The membrane separation is typically referred to separation technology based on a semipermeable or selective membrane.[2,8] The membrane performance in a gas separation process is basically determined with two parameters, selectivity and permeability. Selectivity is the capability of a membrane to selectively separate a desired molecule from a mixture. Whereas, permeability shows the membrane's productivity per unit time.[9] An ideal membrane, for gas separation purposes, should have a low diffusion barrier for a specific type of molecule (permeability) and high diffusion barrier for other components within the gas mixture (selectivity). Apparently, a membrane with high selectivity usually suffers from low permeability, and *vice versa*.[10] Therefore, there is always an intercommunication between selectivity and permeability of a membrane.

Traditional membranes for gas separation, like polymers,[11] metals,[12] zeolites,[13] silica,[14] and metal organic frameworks[15] do not possess both high permeability and selectivity. Carbonaceous materials can be considered as very promising

[a]*Department of Chemistry and Molecular Biology, University of Gothenburg, 405 30 Göteborg, Sweden. E-mail: sayyed.jalil.mahdizadeh@gu.se*

[b]*Department of Chemistry, Ferdowsi University of Mashhad, Mashhad 9177948974, Iran*

† Electronic supplementary information (ESI) available: The Morse potential parameters for interaction between various gas molecules and different membranes, optimized unit cell of different membranes, and .xyz file format of graphdiyne, graphenylene, and rhombic-graphyne membranes. See DOI: 10.1039/d0ra04286b

membranes in gas separation processes, since carbon is an abundant element and its allotrope's production techniques have been widely evaluated.[9] It has been proven that the membrane permeability inversely correlates with its thickness.[16] Therefore, porous 2D graphene-based nanomaterials, with one-atom thickness, have fascinated a great attention as efficient membranes for gas and liquid separation and purification processes.[17–21]

The pristine graphene is totally impermeable to any kind of gases even tiny He molecules.[22] Hence, making in-plane pores in graphene sheets is necessary to attain molecular permeability. However, carving perfect and precise nanopores at large density level on a graphene sheet is extremely tricky and needs advanced breakthroughs in nano-scale manufacturing technologies.[23] Therefore, finding novel 2D membranes with intrinsic uniform nanopores with specific architecture is essential as an alternative route. Graphenylene is an interesting allotrope of graphene with all the $sp^2$-hybridized carbon atoms which was firstly suggested by Balaban *et al.*[24] Graphenylene has attracted a great attention because of its thermal and mechanical stability and especially periodic unique pore architecture.[25–27] Recently, some research groups could successfully synthesize graphenylene.[3,28] Similar to graphene and graphenylene with purely $sp^2$-hybridized network, other advanced 2D carbonaceous nanomaterials with successive $sp^2$- sp-hybridized carbon atoms have been hypothesized theoretically.[29] For example, the graphyne family can be built by replacing 1/3 of C–C bonds in graphene with n-acetylene linkages (–C≡C–) ($n$ = 1, 2, 3, …) which would produce graphyne, graphyne-2 (graphdiyne), graphyne-3, *etc.*, respectively.[30] Interestingly, some experimental techniques have been employed to successfully produce graphynes family.[31–33] On the other hand, replacement of 2/3 of C–C bonds in graphene with acetylene linkage will produce a new 2D layered carbon allotrope called rhombic-graphyne.[34]

Due to the precise and uniform pore structure of these 2D nanomaterials, they are considered as promising ideal membrane for gas separation and purification.[35] Jiao *et al.*[36] evaluated the potential application of graphdiyne as membrane to separate $H_2$ from syngas. According to their findings, graphdiyne shows a $H_2$ permeability about $10^4$ times greater than that of porous graphene. Zhao *et al.*[37] investigated the selective separation of different light gases by H-, O-, and F-substituted graphdiyne using computational approaches. They found that O- and F-substituted graphdiyne could efficiently separate $CH_4$ and $N_2$ gases. Cranford *et al.*[38] estimated the flux of $H_2$ passing through the graphdiyne membrane to be 7–10 g $cm^{-2}$ $s^{-1}$ from a gas mixture containing $CH_4$ and CO molecules. Employing the first principle calculations, Zhang[35] studied the $H_2$ separation features of graphynes family over light gas molecules (*e.g.* $CH_4$, $N_2$, CO). According to their results, graphyne was not a suitable membrane for $H_2$ separation because of its small pore size. However, graphdiyne demonstrated a high selectivity for $H_2$ molecules ($10^9$) over bigger molecules like $CH_4$ but relatively low selectivity ($10^3$) over smaller molecules. In addition, they showed that rhombo-graphyne has an extremely high selectivity for $H_2$ molecules ($10^{16}$) over other light gases. Zhang *et al.*[39] showed that some graphyne derivatives, with pore sizes of 7 × 8 Å, could effectively blocks both di-branched and mono-branched pentane isomers. Using the dispersion-corrected DFT calculations, Zhu *et al.*[1] estimated the separation performance of light gas mixtures *via* strained-control graphenylene. Their results indicated that applying lateral strain has a notable impact on the separation performance and selectivity of graphenylene membrane.

Herein, using dispersion corrected DFT calculations (DFT-D3) and non-equilibrium molecular dynamics simulation (NEMD), we have evaluated the selective separation performance of Graphdiyne (GD), Graphenylene (GN), and Rhombo-Graphyne (RG) for multicomponent mixture of light gases including $H_2$, $N_2$, $O_2$, $CO_2$, and $CH_4$ molecules.

## Methods

### Quantum mechanics calculations

The quantum mechanics calculations were performed using Quantum ESPRESSO package.[40] All geometry optimizations were carried out based on the periodic variable-cell plane-wave DFT calculations with the generalized gradient approximation (GGA) using Perdew–Burke–Ernzerhof (PBE) functional.[41] The ultrasoft pseudopotential prepared through the Rappe–Rabe–Kaxiras–Joannopoulos scheme[42] was used to model the ionic cores. The kinetic cutoff for charge densities and wave functions were defined to 4000 and 400 eV, respectively. The Brillouin zone integration was performed by an 8 × 8 × 1 Monkhorst–Pack grid.[43] The convergence procedure was enhanced by applying Marzari–Vanderbilt cold smearing with 0.95 eV of broadening parameter.[44] A vacuum gap with 20 Å thickness was considered in $z$-direction to minimize the interaction between periodic images. During the structural optimization process, the positions of all atoms in the unit-cell were fully relaxed until the convergence criteria of $1 \times 10^{-4}$ eV for total energies and $1 \times 10^{-3}$ eV $Å^{-1}$ for forces were met. Also, the criterion for self-consistent field calculation was set to be $1 \times 10^{-5}$ eV.

The Climbing Image Nudged Elastic Band (CI-NEB) method[45] was used with dispersion-corrected DFT calculations (DFT-D3),[46] as implemented in the Quantum ESPRESSO package, to investigate the minimum energy pathways (MEPs) of various gas molecules passing through the different membranes and to extract the interaction potential function parameters. The path threshold for CI-NEB calculations was set to 0.05 eV $Å^{-1}$ and 20 points were defined to discretize the path.

### NEMD simulations

For non-equilibrium molecular dynamics (NEMD) simulation, the structurally optimized membranes with area of about 158 $nm^2$ were placed in the middle of the permeate and feed sides. The feed side of the simulation box was filled up with 2000 gas molecules from each type, while the permeate side was set to be empty. Two rigid sheets of graphene were used as pistons to apply external pressure on the permeate and feed chambers. During the NEMD simulation, all the membranes were

 

considered as rigid body because it has been stablished that the flexibility of the membrane has insignificant effect on the outputs.[47] Also, it has been demonstrated that graphyne derivatives are much more rigid than other porous 2D materials like porous graphene and porous boron nitride membranes.[39] Besides, the main goal of this study is to estimate the gas permeability at low pressure using linear interpolation of discrete data, where the possible membrane's distortion is at its minimum level.

All NEMD simulations were carried out by LAMMPS package.[48] The velocity Verlet scheme was employed with time step of 0.5 fs to integrate the equation of atomic motions. The periodic boundary conditions were also applied in $X$ and $Y$ directions. The simulation box was first fully equilibrated for 2 ns in the NVT ensemble (Nose–Hoover thermostat) with a fixed 1 atm pressure exerted on both pistons along the $Z$ direction. Afterwards, the production run was lunched in the NEMD scheme along with applying 100–700 MPa pressure on the feed's piston (Fig. 3). In NEMD scheme, exerting much higher pressure than that practically applied is utterly prevalent to elevate the signal-to-noise ratio and minimize thermal noises within a short timescale.[49] To apply pressure ($P$), defined amount of force ($F$) was exerted on every individual atoms of the piston based on the equation, $F = (P \times A)/n$, where $A$ and $n$ are the piston area and the number of atoms, respectively. Both pistons were free to move along the $Z$ direction to reach the desired pressure.

The interaction energy between gas molecules and different membranes were extracted from quantum mechanics calculations and modeled using the Morse potential function as will discuss in the next section. The COMPASS force field[50,51] was employed to describe both bonded and non-bonded interactions of gas molecules with 15 Å cutoff for van der Waals forces. Coulomb's law was employed for short-range coulombic interactions within a cutoff radius of 15 Å, while, PPPM technique[52] was considered for long-range coulombic interaction.

## Results and discussion

### Quantum mechanics calculations

For the first step, the 2D structures of GD, GN, and RG were optimized by means of variable-cell DFT calculations. The optimized structures of the membranes used in the current study are shown in Fig. 1 where the dashed area confined between two lattice vectors $\vec{a}$ and $\vec{b}$ represents the unit cells. The

Table 1 The calculated cell lattice parameters of GD, GN, and RG from this work and those from the literature given in the parentheses

| Membrane | $a$ (Å) | $b$ (Å) | $\alpha$ (°) |
|---|---|---|---|
| GD | 9.43 (9.48),[53] (9.39)[35] | 9.43, (9.48),[53] (9.39)[35] | 120 (120)[53] |
| GN | 6.74, (6.76)[53] | 6.74, (6.76)[53] | 60 (60)[53] |
| RG | 6.97, (6.91)[1] | 6.88, (6.84)[1] | 90 (90)[1] |

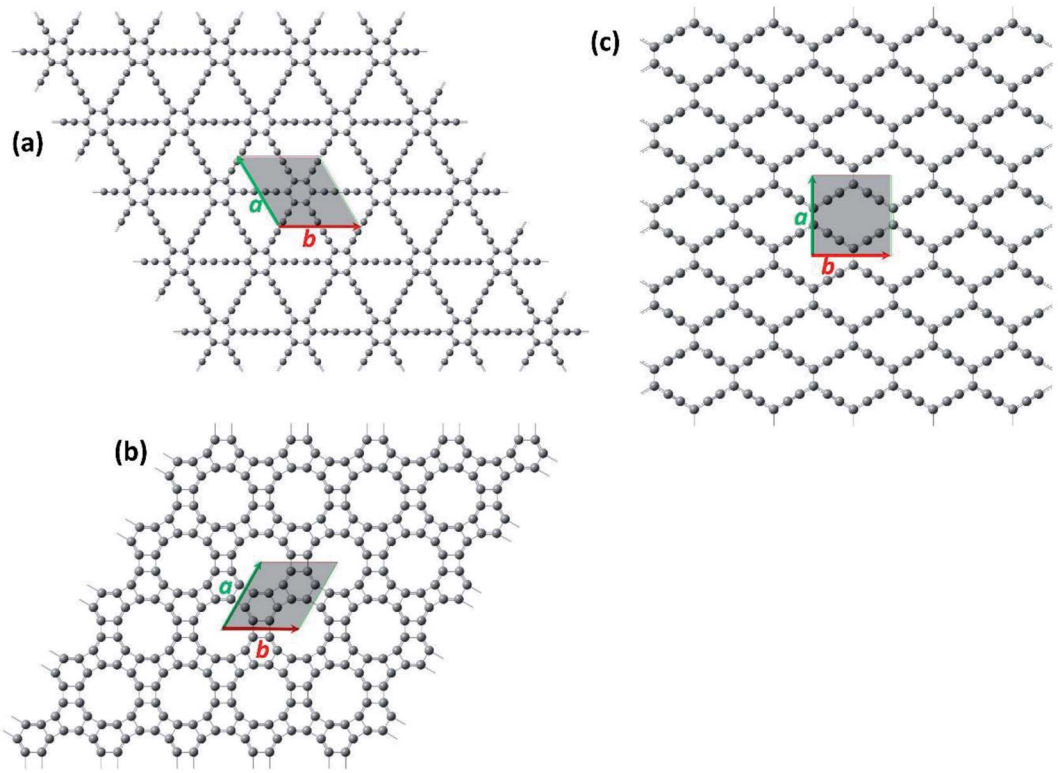


Fig. 1 The optimized structure of (a) Graphdiyne (GD), (b) Graphenylene (GN), and (c) Rhombo-Graphyne (RG). The dashed area confined between two lattice vectors $\vec{a}$ and $\vec{b}$ represents the unit cells.

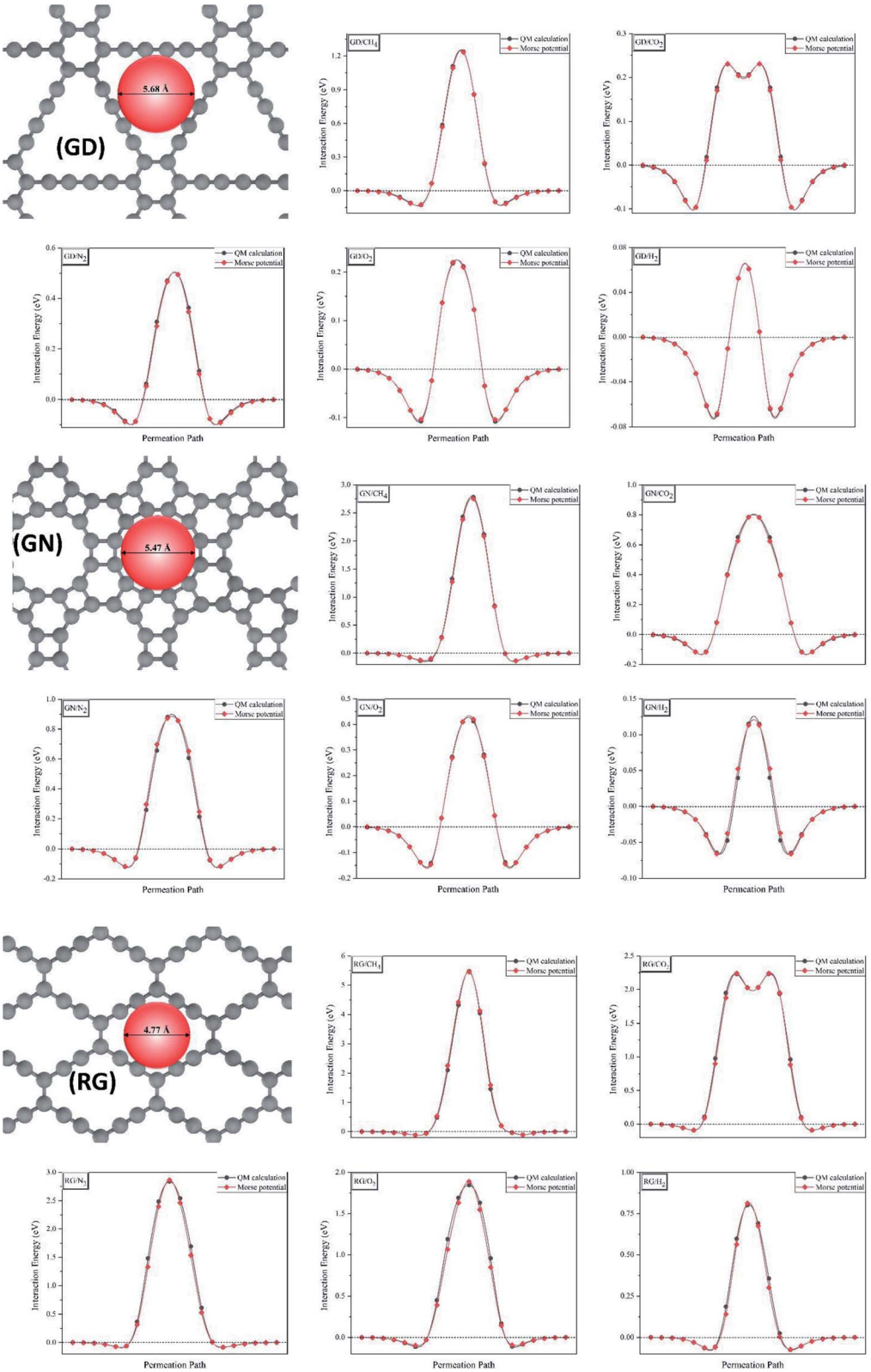


Fig. 2 The interaction energy of various gas molecules passing through the different membranes calculated using CI-NEB and those fitted to the Morse potential. The van der Waals pore diameter of each membrane are presented by red spheres.

 

coordinates for optimized unit cells of different membranes are provided in the ESI.† The calculated cell lattice parameters are also presented in Table 1. As this table indicates, there is a very good agreement between lattice parameters calculated in this work and those reported in the literature. These results confirm that the calculated structures are accurate enough to provide a precise insight about the hole size and morphology of the membranes.

Afterwards, CI-NEB calculations were employed to investigate the MEPs of various gas molecules passing through the different membranes (Fig. 2) and to extract the interaction potential function parameters. The interaction energy between membrane surface and gas molecules, $E$, were calculated for 20 points which were used to discretize the MEP. Then, chi-square minimization technique was used to fit these points into the Morse potential (eqn (1)) by generalized reduced gradient algorithm.[54]

$$E = D_0[e^{-2\alpha(r-r_0)} - 2e^{-\alpha(r-r_0)}] \quad (1)$$

where $r_0$, $D_0$, and $\alpha$ are equilibrium distance (Å), well's width controller ($Å^{-1}$), and potential well depth (eV), respectively. $r$ is the distance between each atom of the adsorbate molecule and each carbon atom of the membrane. In practice, the distance between all atoms of the adsorbate molecule and all carbon atoms of the membrane were calculated at every 20 points of MEP. Then, the interaction energy calculated from the DFT CI-NEB was fitted into the summation over all the pairwise interactions. During the CI-NEB calculations and minimization process, the membrane was considered big enough to make it possible to sample all pairwise interactions within the cutoff radius of 10 Å, *i.e.* the total interaction energy doesn't change for a bigger membrane.

Fig. 2 shows the interaction energy of various gas molecules permeating through the different membranes calculated using CI-NEB and those fitted to the Morse potential. As this figure shows, the Morse potential fits very good at both attraction and repulsion regions. Table 2 compares the energy barriers for different gas molecules calculated using CI-NEB and those predicted from Morse potential. As one can see from Table 2, the difference between two energy barriers is less than 2% for all diffusing gas molecules. According to these results, the Morse potential could precisely reproduce the interaction energies and could be considered as a perfect bridge between quantum mechanics calculations and molecular dynamics simulation in this work. It has been approved that Morse potential can accurately describe the non-bonded interactions calculated by high level quantum mechanics techniques.[55] The Morse potential parameters for interaction between various gas molecules and different membranes are shown in Table S1.†

Table 3 The selectivity of different membranes for each gas pairs

| $S_{\frac{Gas_1}{Gas_2}}$ | GD | GN | RG |
|---|---|---|---|
| $H_2/CH_4$ | $5 \times 10^{19}$ | $2 \times 10^{44}$ | $9 \times 10^{77}$ |
| $H_2/CO_2$ | $7 \times 10^{2}$ | $2 \times 10^{11}$ | $1 \times 10^{24}$ |
| $H_2/N_2$ | $2 \times 10^{7}$ | $6 \times 10^{12}$ | $3 \times 10^{34}$ |
| $H_2/O_2$ | $5 \times 10^{2}$ | $1 \times 10^{5}$ | $1 \times 10^{18}$ |
| $O_2/CH_4$ | $1 \times 10^{17}$ | $2 \times 10^{39}$ | $7 \times 10^{59}$ |
| $O_2/CO_2$ | 1.4 | $1 \times 10^{6}$ | $8 \times 10^{5}$ |
| $O_2/N_2$ | $4 \times 10^{4}$ | $5 \times 10^{7}$ | $2 \times 10^{16}$ |
| $CO_2/CH_4$ | $8 \times 10^{16}$ | $1 \times 10^{33}$ | $9 \times 10^{53}$ |
| $CO_2/N_2$ | $3 \times 10^{4}$ | 32.5 | $3 \times 10^{10}$ |
| $N_2/CH_4$ | $3 \times 10^{12}$ | $4 \times 10^{31}$ | $3 \times 10^{43}$ |

The membrane selectivity for one gas ($Gas_1$) over other gases ($Gas_2$) can be estimated based on the Arrhenius equation:[52]

$$S_{\frac{Gas_1}{Gas_2}} = \frac{D_{Gas_1}}{D_{Gas_2}} = \frac{A_{Gas_1}\exp\left(-\frac{E_{Gas_1}}{RT}\right)}{A_{Gas_2}\exp\left(-\frac{E_{Gas_2}}{RT}\right)} \quad (2)$$

where $A$, $D$, $T$ and $E$ are the diffusion pre-factor, diffusion rate, absolute temperature, and diffusion energy barrier, respectively. Assuming that the passing-through processes of all gases follow the Arrhenius equation with the same pre-exponential factors[39] and $T = 300$ K, the selectivity of membranes for each gas pairs can be calculated. The results are presented in Table 3. According to the selectivity results, the possibility of separating a mixture of gases can be examined by means of new membranes introduced here: For GD, the highest selectivity values belong to gas/$CH_4$ pairs (gas = $H_2$, $O_2$, $CO_2$, and $N_2$) which implies $CH_4$ molecules can be separated from the mixture using GD as membrane. For GN, the separation selectivity values for gas/$CO_2$ and gas/$N_2$ (gas = $H_2$ and $O_2$) are also high. Therefore, GN membrane seems to be able to separate $H_2$ and $O_2$ from the remaining gas mixture. On the other hand, the selectivity of $H_2/O_2$ on RG is high enough ($1 \times 10^{18}$) to

Table 2 Energy barriers (eV) for gas molecules passing through the different membranes calculated using QM and those predicted from Morse potential and the absolute relative difference between these two values (Rel.)

| | GD | | | GN | | | RG | | |
|---|---|---|---|---|---|---|---|---|---|
| | Morse | QM | Rel. (%) | Morse | QM | Rel. (%) | Morse | QM | Rel. (%) |
| $CH_4$ | 1.240 | 1.235 | 0.4 | 2.781 | 2.754 | 1.0 | 5.475 | 5.451 | 0.4 |
| $CO_2$ | 0.231 | 0.230 | 0.4 | 0.784 | 0.782 | 0.3 | 2.232 | 2.240 | 0.3 |
| $N_2$ | 0.494 | 0.494 | 0.0 | 0.880 | 0.872 | 0.9 | 2.838 | 2.864 | 0.9 |
| $O_2$ | 0.218 | 0.221 | 1.4 | 0.412 | 0.415 | 0.7 | 1.855 | 1.888 | 1.7 |
| $H_2$ | 0.061 | 0.061 | 0.0 | 0.115 | 0.113 | 1.8 | 0.801 | 0.812 | 1.3 |

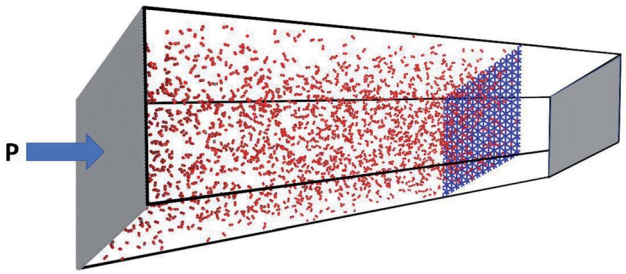


Fig. 3 Snapshot of the simulation box after the initial 2 ns equilibrium stage. Two pistons and membrane are illustrated in grey and blue, respectively.

anticipate that RG membrane can separate $H_2$ and $O_2$ molecules. However, using the Arrhenius equation to calculate the membrane selectivity is just an estimation because there are two major approximations: (1) the driving force for diffusion barrier is electronic energy not enthalpy, (2) the entropy contribution is included within the pre-factors which were assumed to be identical for each gas. Therefore, a series of extensive NEMD simulation were conducted to gain more realistic insight regarding the separation selectivity and gas permeation through the various membranes.

### Non-equilibrium MD simulation

To gain realistic insight about selectivity and gas permeability of different membranes, a series of NEMD simulation were performed as describes in computational details section. Fig. 3 shows a snapshot of the simulation box after 2 ns equilibration, where two pistons (graphene sheets) and membrane (GD) is illustrated in grey and blue respectively. The NEMD simulation results approved that none of the membranes are permeable for $CH_4$ molecules. On the other hand, GN and RG are impermeable for $N_2$ and $CO_2$ molecules, while they can pass through the GD membrane.

Fig. 4 shows the number of gas molecules ($N_{gas}$, gas = $N_2$ and $CO_2$) passing through the GD as a function of applied pressure ($P$) and time ($t$). While both $N_{N_2}$ and $N_{CO_2}$ increase almost linearly with time, the rates of increase, at constant pressure, is much higher for $CO_2$ gas. For example, at 500 MPa, $N_{N_2}$ and $N_{CO_2}$ reach to 200 after 26 and 5.5 ns, respectively. In addition, Fig. 4

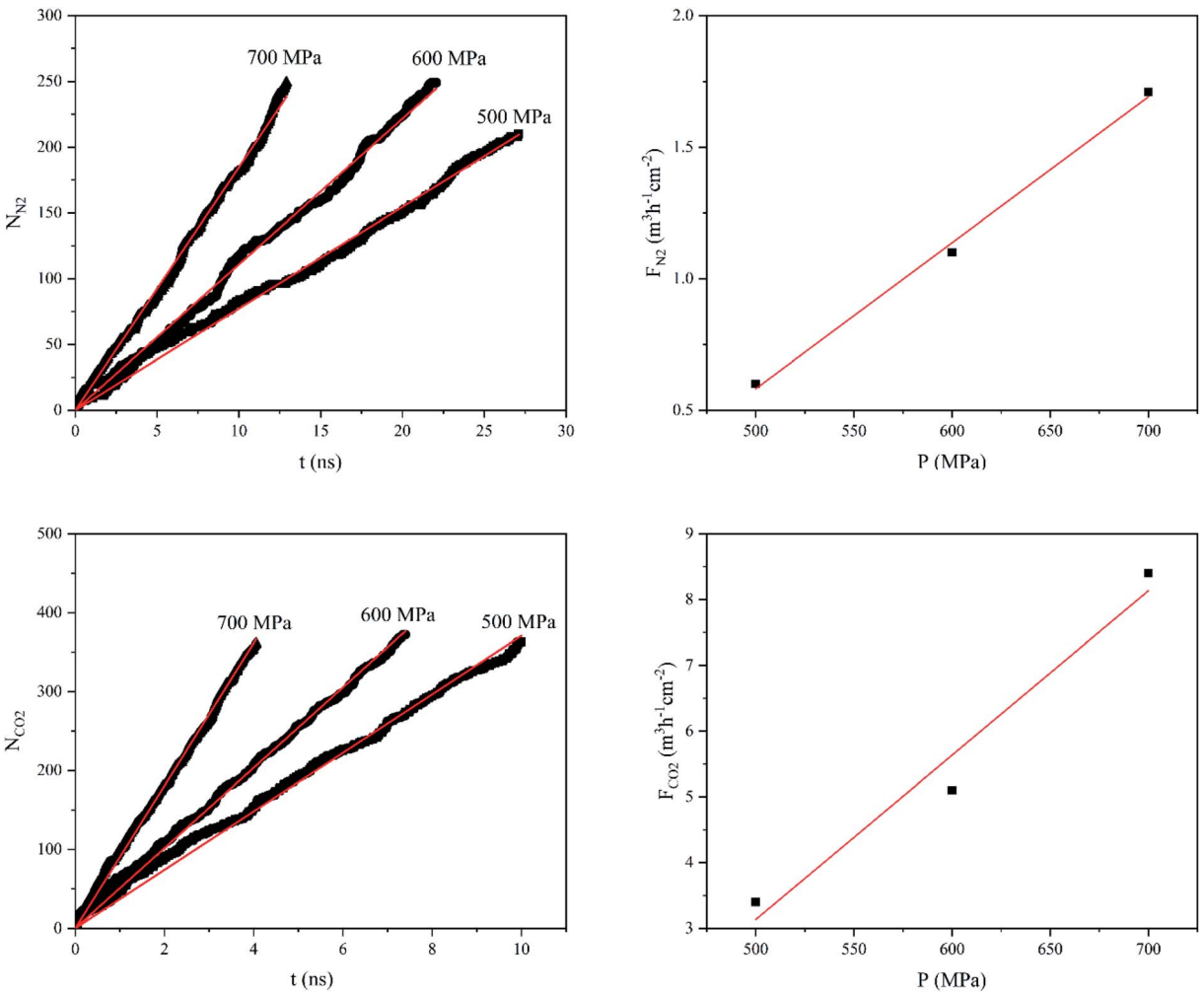


Fig. 4 Number of $N_2$ and $CO_2$ molecules ($N_{gas}$) passing through the GD a function of time ($t$), and gas flux ($F_{gas}$) as a function of exerted pressure ($P$).

 

illustrates the gas flux ($F_{gas}$, gas = $N_2$ and $CO_2$) as a function of applied pressure. As one can see, there is also a linear correlation between gas flux and applied pressure. Hence, the gas permeability can be estimated from the slope of the linear plot $F_{gas}$ *vs. P*. The gas permeability values of GD membrane for $CO_2$ and $N_2$ gases were calculated to be 25.1 and 5.5 L $h^{-1}$ $cm^{-2}$ $MPa^{-1}$ (at STP), respectively.

According to the NEMD simulation results, oxygen molecules are able to diffuse through the GD and GN membranes but not RG. Fig. 5 shows the $N_{O_2}$ and $F_{O_2}$ values of GD and GN membranes as a function of applied pressure and time. The number of oxygen molecules passing through both GD and GN membranes increases almost linearly with time. However, at the constant pressure, $N_{O_2}$ for GD is much higher than that of GN. For instance, at 500 MPa, $N_{O_2}$ reaches to 300 after 5.4 and 25 ns for GD and GN membranes, respectively. The $O_2$ gas permeability values were estimated to 29.3 and 9.8 L $h^{-1}$ $cm^{-2}$ $MPa^{-1}$ (at STP) for GD and GN membranes, respectively.

Hydrogen molecules, due to the smallest size, can pass through all different types of membranes. Fig. 6 shows the $N_{H_2}$ and $F_{H_2}$ values of GD, GN, and RG membranes. NEMD simulations show that, at the constant applied pressure, the number of $H_2$ molecules diffusing through the RG is significantly lower than those of GD and GN membranes. For example, at 300 MPa, the time elapsed for $N_{H_2}$ to reach 1000 was 0.15, 0.26, and 2.0 ns for GD, GN, and RG membranes respectively. The calculated $H_2$ gas permeability values were calculated to be 2180.1, 1070.5, and 160.2 L $h^{-1}$ $cm^{-2}$ $MPa^{-1}$ (at STP) for GD, GN, and RG membranes, respectively.

The NEMD simulation results gave us the following insights: (1) methane molecules can be separated from the other gases (*i.e.* $H_2$, $O_2$, $CO_2$, $N_2$) using the GD as membrane (2) none of the membranes can completely separate $CO_2$ and $N_2$ molecules. However, the permeability of $CO_2$ molecules through the GD membrane is ~5 times greater than that of $N_2$ molecules. (3) $O_2$ and $H_2$ can be separated from other gases by means of GN membrane. (4) $H_2$ and $O_2$ molecules can be separated perfectly

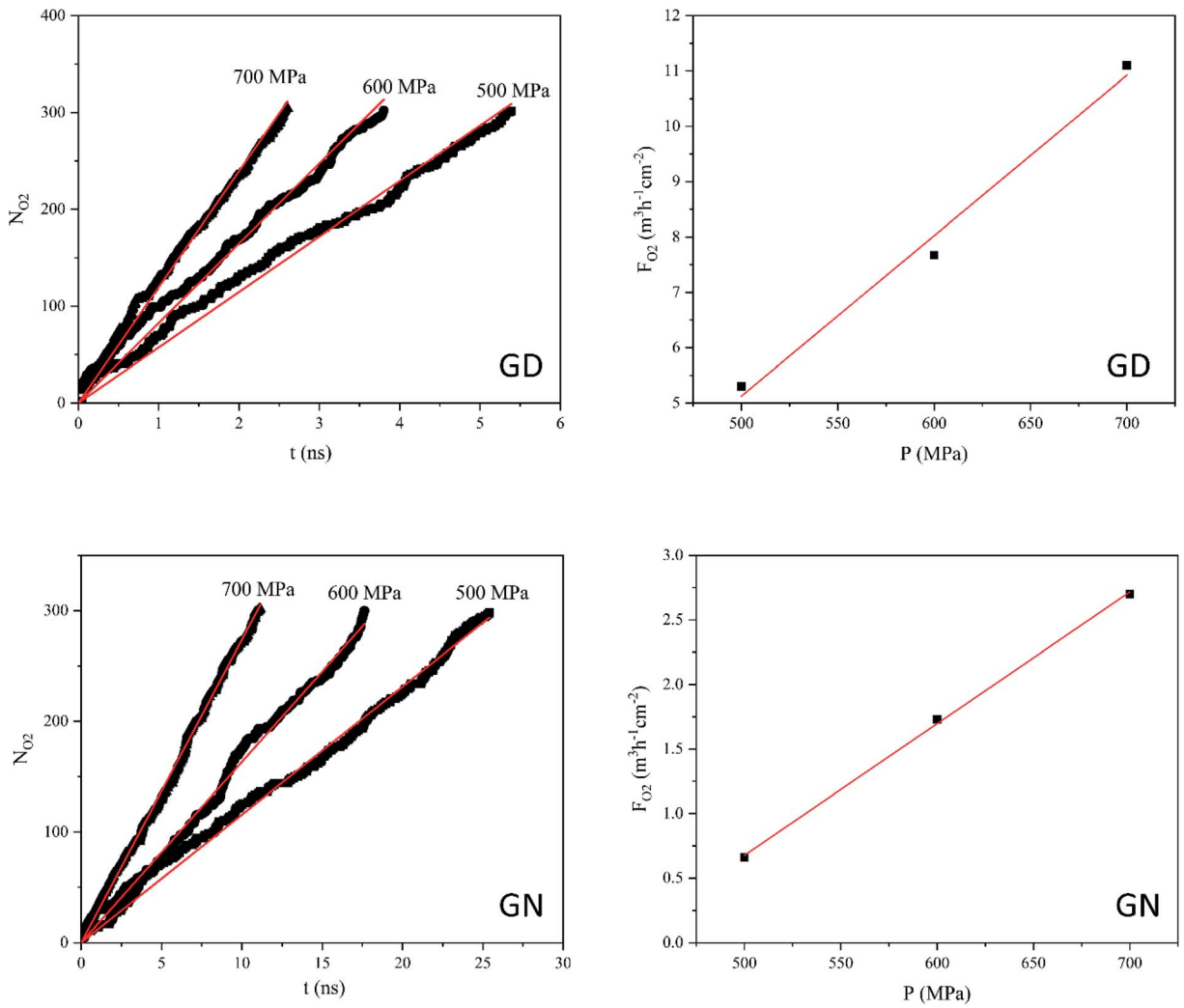


Fig. 5 Number of $O_2$ molecules ($N_{O_2}$) passing through the GD and GN membranes as a function of time ($t$) and, and $O_2$ flux ($F_{O_2}$) as a function of exerted pressure ($P$).

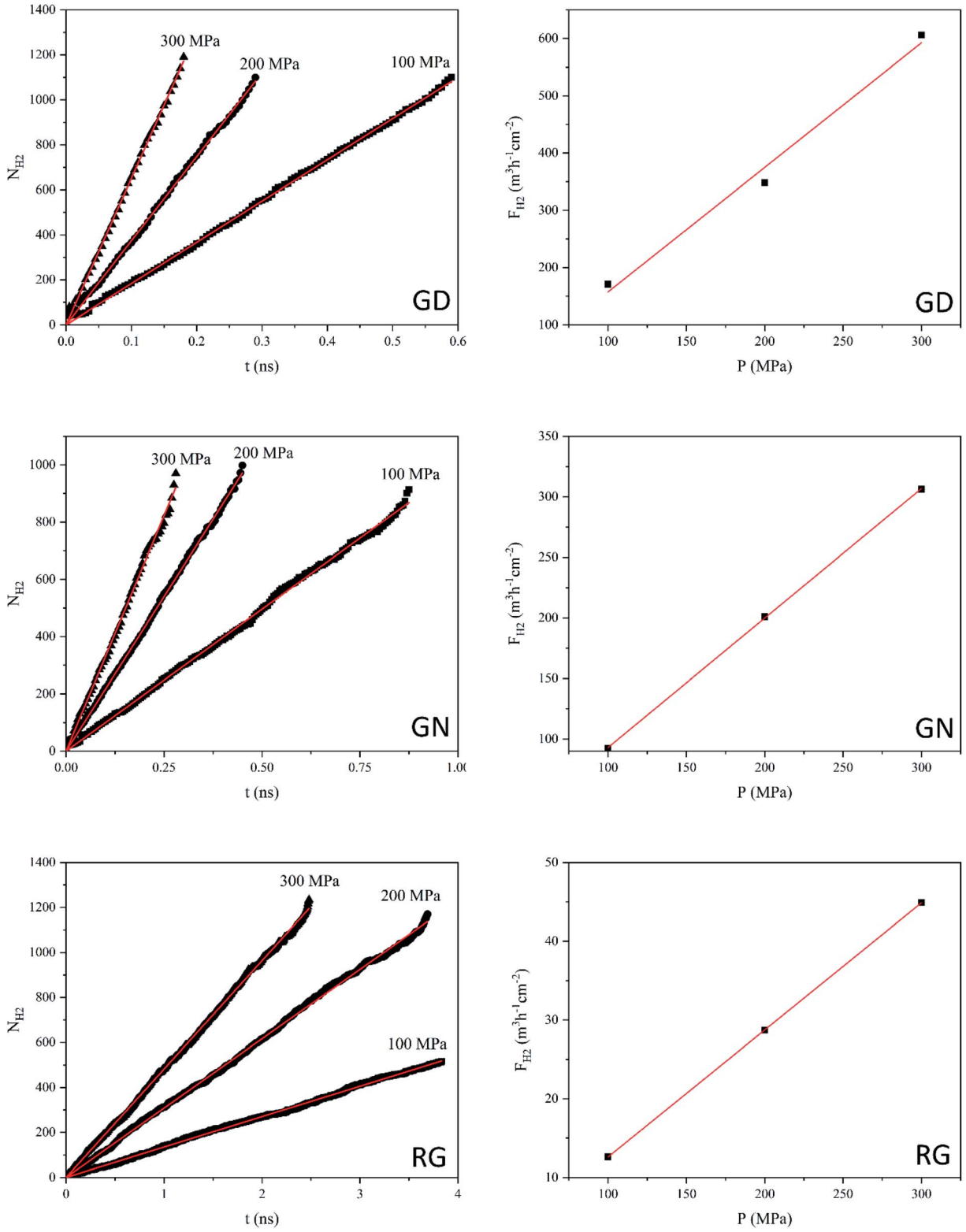


Fig. 6 Number of $H_2$ molecules ($N_{H_2}$) passing through the GD, GN, and RG membranes as a function of time, and $H_2$ flux ($F_{H_2}$) as a function of exerted pressure ($P$).

using RG membrane. (5) the NEMD simulation results are generally consistent with the selectivity data calculated from Arrhenius equation. However, after analyzing the NEMD data and comparing the results with Arrhenius selectivity values, the limitation of the Arrhenius equation for prediction of the true selectivity was clearly revealed. For example, RG membrane is

 

totally impermeable for all gases except $H_2$, but Arrhenius predicts a very high selectivity for $O_2/CH_4$ ($\sim 10^{60}$), $CO_2/CH_4$ ($\sim 10^{54}$), and $N_2/CH_4$ ($\sim 10^{43}$). It is because the selectivity value based on the Arrhenius equation depends on the difference between the diffusion barrier energies of each gas and not the absolute values. Therefore, a membrane can be impermeable for both gases (with very different barrier energies) while the Arrhenius shows a very high selectivity.

## Conclusions

Herein, we employed multiscale computational approach, combining plane-wave DFT calculations and extensive NEMD simulation, to investigate the possibility of multicomponent low weight gas ($H_2$, $O_2$, $N_2$, $CO_2$, $CH_4$) separation and purification using novel porous 2D carbonaceous nanomaterials, namely Graphdiyne (GD), Graphenylene (GN), and Rhombic-Graphyne (RG). The results indicated that $CH_4$ molecules are not able to pass through any of these membranes while $CO_2$ and $N_2$ molecules can just pass through DG membrane. The calculated permeability values of GD membrane for $CO_2$ and $N_2$ molecules are 25.1 and 5.5 L $h^{-1}$ $cm^{-2}$ $MPa^{-1}$ (at STP), respectively. $O_2$ molecules can pass through GD and GN membranes with the corresponding permeability values of 29.3 and 9.8 L $h^{-1}$ $cm^{-2}$ $MPa^{-1}$ (at STP), respectively. On the other hand, $H_2$ molecule can diffuse through all membranes with estimated permeability values of 2180.1, 1070.5, and 160.2 L $h^{-1}$ $cm^{-2}$ $MPa^{-1}$ (at STP) for GD, GN, and RG membranes, respectively. This study shows that $CH_4$ molecules can be completely separated from the other gases using GD membrane, $O_2$ molecules from $CH_4$, $N_2$, and $CO_2$ by GN membrane, and $H_2$ molecules from all other gases using RG membrane. However, it seems complete separation of $CO_2$ and $N_2$ molecules is not possible with three membranes studied here. According to the results, graphdiyne, graphenylene, and rhombic-graphyne nanomaterials are promising membranes for multicomponent gas separation and purification.

## Conflicts of interest

There are no conflicts to declare.

## Acknowledgements

Authors acknowledge financial support from Iran Science Elites Federation (ISEF). Exclusive support from Prof. Leif A. Eriksson (University of Gothenburg) is greatly appreciated.

## References

1 L. Zhu, Y. Jin, Q. Xue, X. Li, H. Zheng, T. Wu and C. Ling, *J. Mater. Chem. A*, 2016, **4**, 15015–15021.
2 S. J. Mahdizadeh and E. K. Goharshadi, *Int. J. Hydrogen Energy*, 2019, **44**, 8325–8340.
3 R. Totani, C. Grazioli, T. Zhang, I. Bidermane, J. Lüder, M. de Simone, M. Coreno, B. Brena, L. Lozzi and C. Puglia, *J. Chem. Phys.*, 2017, **146**, 054705.
4 J. G. Vitillo, B. Smit and L. Gagliardi, *Chem. Rev.*, 2017, **117**, 9521–9523.
5 M. Shan, B. Seoane, E. Rozhko, A. Dikhtiarenko, G. Clet, F. Kapteijn and J. Gascon, *Chem.–Eur. J.*, 2016, **22**, 14467–14470.
6 N. F. Himma, A. K. Wardani, N. Prasetya, P. T. Aryanti and I. G. Wenten, *Rev. Chem. Eng.*, 2019, **35**, 591–625.
7 Y. Jiao, A. Du, S. C. Smith, Z. Zhu and S. Z. Qiao, *J. Mater. Chem. A*, 2015, **3**, 6767–6771.
8 H. Ye, D. Li, X. Ye, Y. Zheng, Z. Zhang, H. Zhang and Z. Chen, *Sci. Rep.*, 2019, **9**, 7380.
9 Y. Jiao, A. Du, M. Hankel and S. C. Smith, *Phys. Chem. Chem. Phys.*, 2013, **15**, 4832–4843.
10 L. M. Robeson, *J. Membr. Sci.*, 2008, **320**, 390–400.
11 Y. Yampolskii, *Macromolecules*, 2012, **45**, 3298–3311.
12 S. Yun and S. T. Oyama, *J. Membr. Sci.*, 2011, **375**, 28–45.
13 N. Kosinov, J. Gascon, F. Kapteijn and E. J. Hensen, *J. Membr. Sci.*, 2016, **499**, 65–79.
14 H. L. Castricum, H. F. Qureshi, A. Nijmeijer and L. Winnubst, *J. Membr. Sci.*, 2015, **488**, 121–128.
15 M. S. Denny Jr, J. C. Moreton, L. Benz and S. M. Cohen, *Nat. Rev. Mater.*, 2016, **1**, 16078.
16 S. Oyama, D. Lee, P. Hacarlioglu and R. Saraf, *J. Membr. Sci.*, 2004, **244**, 45–53.
17 L. Huang, M. Zhang, C. Li and G. Shi, *J. Phys. Chem. Lett.*, 2015, **6**, 2806–2815.
18 D.-e. Jiang, V. R. Cooper and S. Dai, *Nano Lett.*, 2009, **9**, 4019–4024.
19 Q. Xu, H. Xu, J. Chen, Y. Lv, C. Dong and T. S. Sreeprasad, *Inorg. Chem. Front.*, 2015, **2**, 417–424.
20 K. Celebi, J. Buchheim, R. M. Wyss, A. Droudian, P. Gasser, I. Shorubalko, J.-I. Kye, C. Lee and H. G. Park, *Science*, 2014, **344**, 289–292.
21 K. Huang, G. Liu, Y. Lou, Z. Dong, J. Shen and W. Jin, *Angew. Chem., Int. Ed.*, 2014, **53**, 6929–6932.
22 J. S. Bunch, S. S. Verbridge, J. S. Alden, A. M. Van Der Zande, J. M. Parpia, H. G. Craighead and P. L. McEuen, *Nano Lett.*, 2008, **8**, 2458–2462.
23 S. J. Mahdizadeh, E. K. Goharshadi and G. Akhlamadi, *Phys. Chem. Chem. Phys.*, 2018, **20**, 22241–22248.
24 A. Balaban, C. C. Rentia and E. Ciupitu, *Rev. Roum. Chim.*, 1968, **13**, 231–247.
25 M. Hankel and D. J. Searles, *Phys. Chem. Chem. Phys.*, 2016, **18**, 14205–14215.
26 Y.-X. Yu, *J. Mater. Chem. A*, 2013, **1**, 13559–13566.
27 Q. Song, B. Wang, K. Deng, X. Feng, M. Wagner, J. D. Gale, K. Müllen and L. Zhi, *J. Mater. Chem. C*, 2013, **1**, 38–41.
28 Q.-S. Du, P.-D. Tang, H.-L. Huang, F.-L. Du, K. Huang, N.-Z. Xie, S.-Y. Long, Y.-M. Li, J.-S. Qiu and R.-B. Huang, *Sci. Rep.*, 2017, **7**, 40796.
29 R. Baughman, H. Eckhardt and M. Kertesz, *J. Chem. Phys.*, 1987, **87**, 6687–6699.
30 L. Pan, L. Zhang, B. Song, S. Du and H.-J. Gao, *Appl. Phys. Lett.*, 2011, **98**, 173102.
31 Q. Li, Y. Li, Y. Chen, L. Wu, C. Yang and X. Cui, *Carbon*, 2018, **136**, 248–254.

32 Y. Li, L. Xu, H. Liu and Y. Li, *Chem. Soc. Rev.*, 2014, **43**, 2572–2586.
33 X. Gao, H. Liu, D. Wang and J. Zhang, *Chem. Soc. Rev.*, 2019, **48**, 908–936.
34 A. N. Enyashin and A. L. Ivanovskii, *Phys. Status Solidi B*, 2011, **248**, 1879–1883.
35 H. Zhang, X. He, M. Zhao, M. Zhang, L. Zhao, X. Feng and Y. Luo, *J. Phys. Chem. C*, 2012, **116**, 16634–16638.
36 Y. Jiao, A. Du, M. Hankel, Z. Zhu, V. Rudolph and S. C. Smith, *Chem. Commun.*, 2011, **47**, 11843–11845.
37 L. Zhao, P. Sang, S. Guo, X. Liu, J. Li, H. Zhu and W. Guo, *Appl. Surf. Sci.*, 2017, **405**, 455–464.
38 S. W. Cranford and M. J. Buehler, *Nanoscale*, 2012, **4**, 4587–4593.
39 L. Zhang, C. Wu, X. Ding, Y. Fang and J. Sun, *Phys. Chem. Chem. Phys.*, 2018, **20**, 18192–18199.
40 P. Giannozzi, S. Baroni, N. Bonini, M. Calandra, R. Car, C. Cavazzoni, D. Ceresoli, G. L. Chiarotti, M. Cococcioni and I. Dabo, *J. Phys.: Condens. Matter*, 2009, **21**, 395502.
41 L. Wang, T. Maxisch and G. Ceder, *Phys. Rev. B: Condens. Matter Mater. Phys.*, 2006, **73**, 195107.
42 A. M. Rappe, K. M. Rabe, E. Kaxiras and J. Joannopoulos, *Phys. Rev. B: Condens. Matter Mater. Phys.*, 1990, **41**, 1227.
43 H. J. Monkhorst and J. D. Pack, *Phys. Rev. B: Solid State*, 1976, **13**, 5188.
44 N. Marzari, D. Vanderbilt, A. De Vita and M. Payne, *Phys. Rev. Lett.*, 1999, **82**, 3296.
45 G. Henkelman, B. P. Uberuaga and H. Jónsson, *J. Chem. Phys.*, 2000, **113**, 9901–9904.
46 S. Grimme, J. Antony, S. Ehrlich and H. Krieg, *J. Chem. Phys.*, 2010, **132**, 154104.
47 H. Daglar and S. Keskin, *J. Phys. Chem. C*, 2018, **122**, 17347–17357.
48 S. Plimpton, *J. Comput. Phys.*, 1995, **117**, 1–19.
49 Z. Hu, Y. Chen and J. Jiang, *J. Chem. Phys.*, 2011, **134**, 134705.
50 H. Sun, *J. Phys. Chem. B*, 1998, **102**, 7338–7364.
51 J. Yang, Y. Ren, A.-m. Tian and H. Sun, *J. Phys. Chem. B*, 2000, **104**, 4951–4957.
52 B. A. Luty and W. F. van Gunsteren, *J. Phys. Chem.*, 1996, **100**, 2581–2587.
53 M. Long, L. Tang, D. Wang, Y. Li and Z. Shuai, *ACS Nano*, 2011, **5**, 2593–2600.
54 L. S. Lasdon, A. D. Waren, A. Jain and M. Ratner, *Design and testing of a generalized reduced gradient code for nonlinear programming*, Stanford Univ Ca Systems Optimization Lab, 1976.
55 L. Yang, L. Sun and W.-Q. Deng, *J. Phys. Chem. A*, 2018, **122**, 1672–1677.